© 2015. Published by The Company of Biologists Ltd | Journal of Cell Science (2015) 128, 2361-2372 doi:10.1242/jcs.168377

RESEARCH ARTICLE

Assembly and maintenance of the flagellum attachment zone filament in *Trypanosoma brucei*

Qing Zhou[1], Huiqing Hu[1], Cynthia Y. He[2] and Ziyin Li[1,*]

ABSTRACT

Adhesion of motile flagella to the cell body in *Trypanosoma brucei* requires a filamentous cytoskeletal structure termed the flagellum attachment zone (FAZ). Despite its essentiality, the complete molecular composition of the FAZ filament and its roles in FAZ filament assembly remain poorly understood. By localization-based screening, we here identified a new FAZ protein, which we called FAZ2. Knockdown of FAZ2 disrupted the FAZ filament, destabilized multiple FAZ filament proteins and caused a cytokinesis defect. We also showed that FAZ2 depletion destabilized another new FAZ filament protein and several flagellum and cytoskeleton proteins. Furthermore, we identified CC2D and KMP11 as FAZ2 partners through affinity purification, and showed that they are each required for maintaining a stable complex. Finally, we demonstrated that FAZ filament proteins are incorporated into the FAZ filament from the proximal region, in contrast to the flagellum components, which are incorporated from the distal tip. In summary, we identified three new FAZ filament proteins and a FAZ filament protein complex, and our results suggest that assembly of the FAZ filament occurs at the proximal region and is essential to maintain the stability of FAZ filament proteins.

KEY WORDS: Flagellum attachment zone, *Trypanosoma brucei*, Flagellum adhesion

INTRODUCTION

Trypanosoma brucei is an early branching protozoan pathogen that causes sleeping sickness in humans and nagana in cattle in Sub-Saharan Africa. A trypanosome cell possesses a single motile flagellum composed of a canonical 9+2 microtubular axoneme and an extra-axonemal structure termed the paraflagellar rod (PFR) (Ralston and Hill, 2008). The flagellum, which is nucleated by the flagellar basal body, exits the cell from the flagellar pocket located at the posterior portion of the cell, and attaches to the cell body along most of its length through the flagellum attachment zone (FAZ), a specialized cytoskeletal structure consisting of a proteinaceous filament (often referred to as the FAZ filament) and a microtubule quartet that associates with the endoplasmic reticulum (Gull, 1999). The FAZ filament mediates flagellum–cell-body attachment and plays an essential role in positioning the cytokinesis cleavage furrow (Gull, 1999; LaCount et al., 2002; Robinson et al., 1995; Vaughan et al., 2008; Zhou et al., 2011). Moreover, elongation of the FAZ filament also controls basal body positioning (Absalon et al., 2007) and cell morphogenesis (Zhou et al., 2011).

[1]Department of Microbiology and Molecular Genetics, University of Texas Medical School at Houston, Houston, TX 77030, USA. [2]Department of Biological Sciences, National University of Singapore, 117543, Singapore.

*Author for correspondence (Ziyin.Li@uth.tmc.edu)

Received 9 February 2015; Accepted 6 May 2015

Adhesion of the flagellum to cell body in trypanosomes appears to involve proteins from both the FAZ filament and the flagellum (Rotureau et al., 2014; Sun et al., 2013; Vaughan et al., 2008; Zhou et al., 2011). FLA1, a putative membrane glycoprotein required for flagellum adhesion in *T. brucei* (LaCount et al., 2002), associates physically with FLA1BP, a recently discovered trans-membrane protein residing on the flagellum membrane (Sun et al., 2013). The C-terminal intracellular domain of FLA1 likely associates with FAZ filament proteins, and the N-terminal extracellular domain of FLA1 interacts with the extra-flagellum domain of FLA1BP, thereby mediating flagellum–cell-body adhesion (Sun et al., 2013). Intriguingly, FLAM3, a new flagellum protein involved in flagellum adhesion, appears to act in the same fashion as the FAZ filament, but on the flagellum side. FLAM3 might constitute a key component of the FAZ connectors that link the axoneme to the FAZ filament (Rotureau et al., 2014). However, it remains unclear whether a FLAM3-containing filament equivalent to the FAZ filament is formed in flagellum along the adhesion zone and whether FLAM3 physically interacts with FLA1BP or any other protein(s) of similar function. Nevertheless, it is clear that flagellum–cell-body adhesion requires extensive interactions between certain structures from both the flagellum and the cell body.

Despite the essential roles of the FAZ filament in flagellum adhesion, the complete molecular composition and the assembly process of the FAZ filament remain poorly defined. To date, nine proteins have been localized to the FAZ filament. Six of them have been functionally characterized, and five of them [with the exception of *T. brucei* (Tb)VAP, also known as Tb927.11.13230] have been found to be essential for FAZ filament assembly and flagellum attachment. Among the nine proteins, FLA1 (also known as Tb927.8.4010) (LaCount et al., 2002), FS179 (also known as Tb927.10.2880) (Oberholzer et al., 2011), TbVAP (Lacomble et al., 2012) and FLA3 (also known as Tb927.5.4570/4580) (Woods et al., 2013) are membrane proteins. Those non-membrane FAZ filament proteins include FAZ1 (Vaughan et al., 2008), CC2D (Zhou et al., 2011) and three hypothetical proteins, which remain to be characterized (Morriswood et al., 2013).

Here, we sought to identify new FAZ filament proteins and investigate how the FAZ filament is assembled and maintained. We identified three new FAZ filament proteins, which we denote FAZ2 (Tb927.1.4310), FAZ8 (Tb927.4.2060) and KMP11 (Tb927.9.13820), and the first FAZ filament protein complex, which was formed by FAZ2, CC2D and KMP11. Furthermore, we demonstrated the requirement of each of the three proteins, FAZ2, CC2D and KMP11, for maintaining a stable complex in the FAZ filament and the requirement of FAZ2 to maintain the stability of certain proteins from the FAZ filament, the flagellum and the cytoskeleton. Finally, we also demonstrated that FAZ filament components are incorporated into the FAZ filament from the proximal base of the FAZ filament near the flagellar pocket, which

Journal of Cell Science (2015) 128, 2361-2372 doi:10.1242/jcs.168377

appears to be opposite orientation to the incorporation of the flagellum components into the flagellum (Bastin et al., 1999).

RESULTS

Identification of FAZ filament proteins by localization-based screening

Previous comparative proteomic studies on pure flagellum and flagellum-associated structures, including the flagellum, basal body, the FAZ and the bilobe structure (Zhou et al., 2010) have identified 223 flagellum-associated proteins, some of which are uncharacterized hypothetical proteins and might be components of the FAZ filament. We hypothesized that the FAZ filament is made of essential large scaffold proteins that form a complex, so we focused on those proteins that have high molecular mass, contain motifs involved in protein–protein interaction, and are essential for cell viability as reported in the previous genome-wide RNA interference (RNAi) screen (Alsford et al., 2011). Based on these criteria, we selected six candidate proteins and determined their subcellular localization by epitope tagging at their endogenous locus. One candidate protein (Tb927.1.4310), which has a predicted molecular mass of 183 kDa and contains four C-terminal coiled-coiled motifs, localized to the FAZ filament (Fig. 1A), as shown by co-localization with FAZ1 and CC2D, two known FAZ filament proteins (Vaughan et al., 2008; Zhou et al., 2011). We named this protein flagellum attachment zone protein 2 (FAZ2) after FAZ1, the first known FAZ filament protein in *T. brucei* (Kohl et al., 1999; Vaughan et al., 2008). FAZ2 appeared to be conserved in *T. cruzi* and *Leishmania*, but no homolog was found outside the kinetoplastids.

FAZ2 RNAi causes flagellum detachment and defective cytokinesis

To investigate the function of FAZ2, RNAi was carried out on the procyclic form. To monitor the efficiency of RNAi, we tagged the endogenous FAZ2 with a triple HA epitope in cells harboring the FAZ2 RNAi construct. Western blotting showed that upon RNAi induction, FAZ2–3HA remained in the cytoskeletal pellet fraction but was gradually reduced to an undetectable level after 48 h of RNAi (Fig. 1B). This depletion of FAZ2 inhibited cell proliferation (Fig. 1C), resulting in the accumulation of cells with multiple (>2) nuclei so that these encompassed ~50% of the total population after RNAi for 72 h (Fig. 1D), suggesting defective cytokinesis. The most striking defect was flagellum detachment, which occurred as early as 16 h after RNAi, and after 48 h more than 80% of the cells contained detached flagella (Fig. 1E). Flagellum detachment occurred on all cell types, including 1N1K (one nucleus and one kinetoplast), 1N2K, 2N2K and polyploid cells.

FAZ2 RNAi disrupts the FAZ filament and destabilizes FAZ filament proteins

Flagellum detachment appeared to be attributed to defective assembly of the new FAZ filament as shown by anti-FAZ1 immunostaining. In all FAZ2-depleted cells with a detached flagellum, FAZ1 was detected at the short new FAZ filament and the full-length old FAZ filament (Fig. 2A), suggesting that FAZ2 is required for assembly of the new FAZ, but not the old FAZ. Due to malformation of the new FAZ filament, we hypothesized that FAZ1 accumulated in the cytosol upon FAZ2 RNAi. To test this

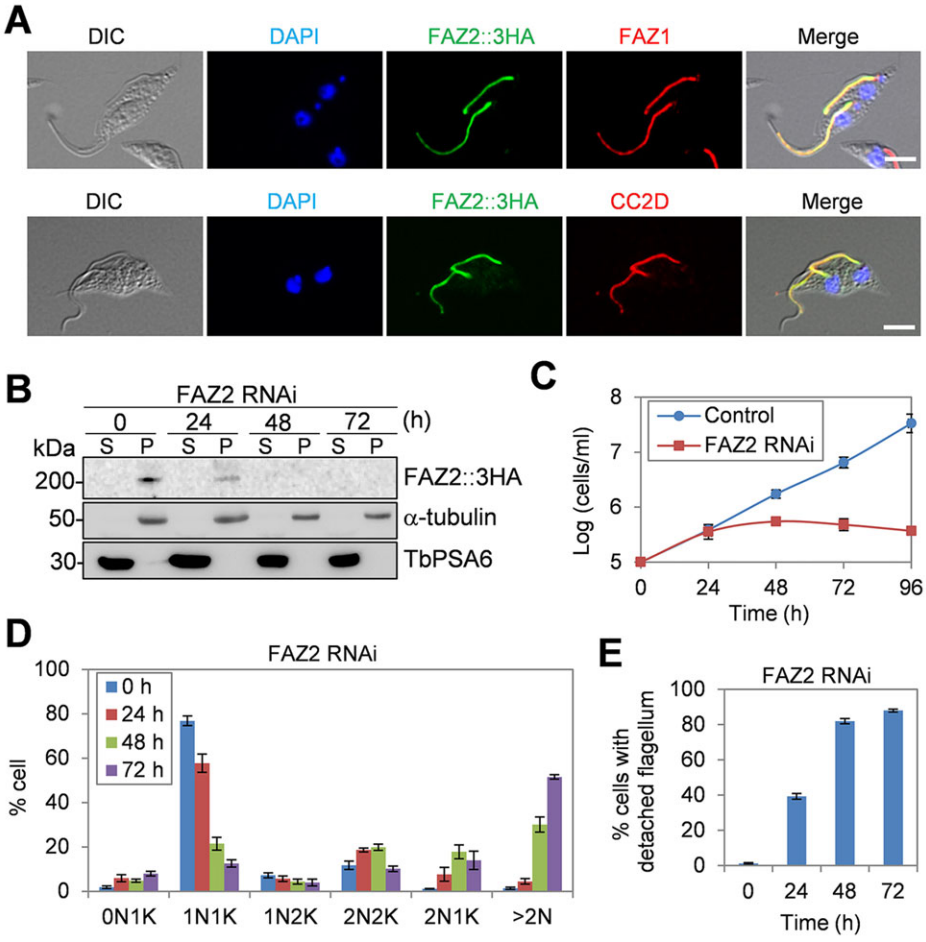

Fig. 1. FAZ2 is a new FAZ protein required for flagellum adhesion. (A) FAZ2 localizes to the FAZ filament. Cells expressing FAZ2–3HA (FAZ2::3HA) were co-immunostained with FITC-conjugated anti-HA mAb and anti-FAZ1 mAb or anti-CC2D pAb. Scale bars: 5 µm. (B) Depletion of FAZ2 by RNAi. FAZ2 was endogenously tagged with a triple HA epitope in cells harboring the FAZ2 RNAi construct. Cells were treated with PEME plus 1% NP40, and cytosolic (S) and cytoskeletal (P) fractions were separated and detected by immunoblotting with anti-HA antibody. The same blot was re-probed with α-tubulin and TbPSA6 as cytoskeletal and cytosolic markers, respectively. S, cytosolic fraction; P, cytoskeletal fraction (C) FAZ2 knockdown inhibits cell proliferation. (D) Quantification of cells with different numbers of nucleus (N) and kinetoplast (K) upon FAZ2 RNAi. Error bars represent s.d. calculated from three independent experiments (n=300). (E) Percentage of cells with detached flagella upon FAZ2 RNAi. Error bars represent s.d. from three independent experiments (n=350).

Journal of Cell Science

Journal of Cell Science (2015) 128, 2361-2372 doi:10.1242/jcs.168377

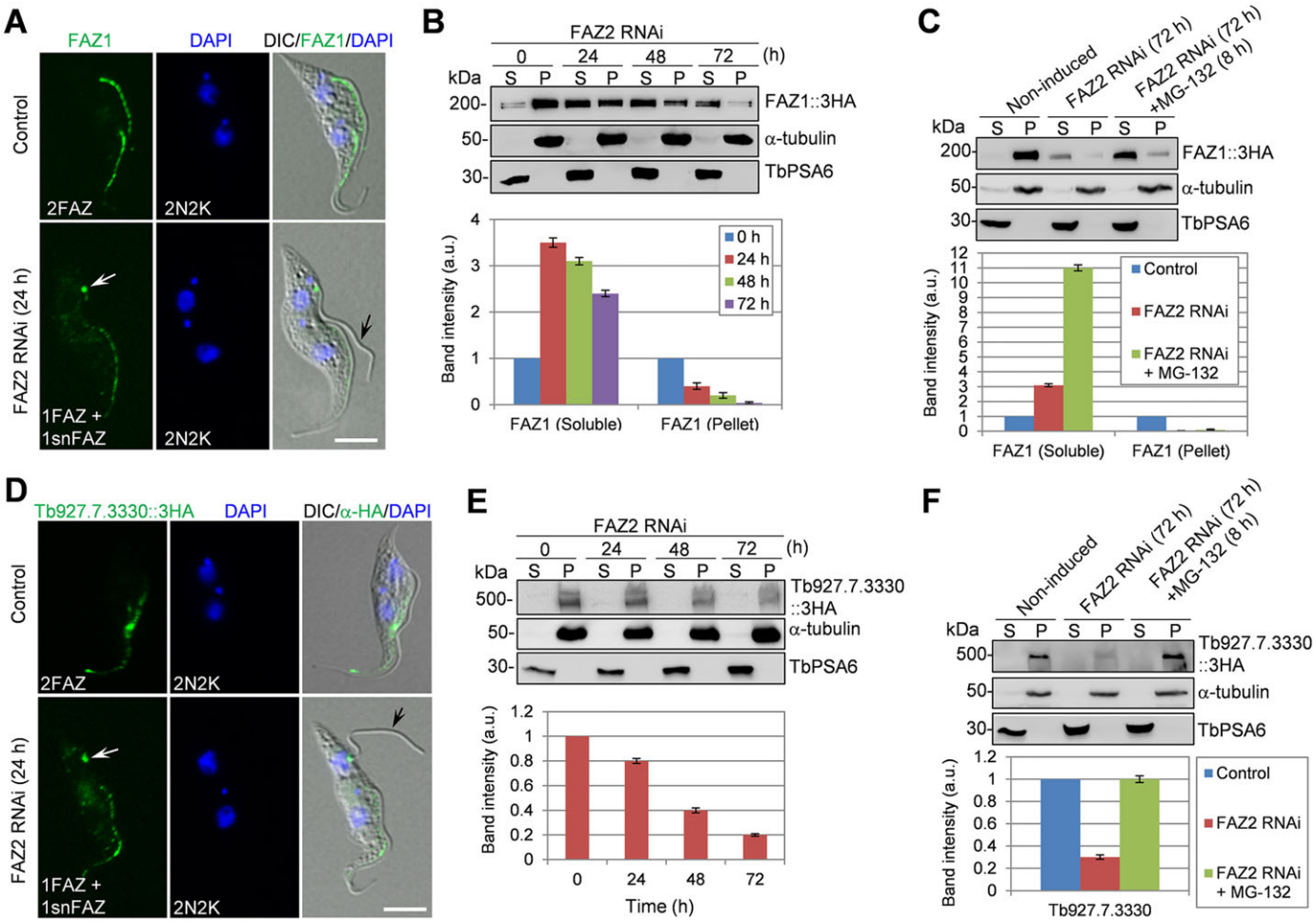

Fig. 2. FAZ2 depletion destabilizes FAZ proteins. (A,D). Immunostaining of FAZ1 and Tb927.7.3330–3HA (Tb927.7.3330::3HA) in control and FAZ2 RNAi cells. Tb927.73330 was tagged at its endogenous locus with a C-terminal triple HA epitope in FAZ2 RNAi cells. White arrows indicate the short new FAZ filament (snFAZ) associated with the detached new flagellum (black arrows). Scale bars: 5 µm. (B,E) Levels of FAZ1 (B) and Tb927.7.3330 (E) in FAZ2 RNAi cells. The two genes were each endogenously tagged with a triple HA epitope in FAZ2 RNAi cells, and detected by anti-HA mAb. The same blot was probed with α-tubulin and TbPSA6 as cytoskeletal and cytosolic markers, respectively. Protein band intensity was determined, normalized to that of loading controls, and plotted as histograms, shown below the western blots. Error bars represent s.d. calculated from three independent experiments. (C,F). Stability of 3HA-tagged FAZ1 and Tb927.7.3330 in FAZ2 RNAi cells. FAZ2 RNAi was induced with tetracycline for 72 h or with tetracycline for 72 h and MG-132 for 8 h. FAZ1 and Tb927.7.3330 were detected by anti-HA mAb. The same blot was re-probed with anti-α-tubulin and anti-TbPSA6, respectively. Protein band intensity was determined as described above. Error bars indicate s.d. calculated from three independent experiments. S, cytosolic fraction; P, cytoskeletal fraction.

possibility, we prepared cytosolic and cytoskeletal fractions for western blotting to monitor the distribution and level of FAZ1, which was endogenously tagged with a triple HA epitope in FAZ2 RNAi cells. FAZ2 RNAi was induced for 24, 48 and 72 h, and western blot was carried out to detect FAZ1 level in the cytosolic and cytoskeletal fractions. The results showed that the FAZ1 level in the cytoskeletal fraction started to decrease after RNAi for 24 h and was reduced to a very low level after 72 h (Fig. 2B). Instead, FAZ1 level in the cytosolic fraction was initially increased after 24 h of RNAi but then gradually decreased (Fig. 2B). Despite this increase in the cytosol, however, the total amount of FAZ1 (in both the cytosolic and cytoskeletal fractions) at 72 h was significantly lower than that in the non-induced control cells (Fig. 2B), suggesting that FAZ1 was probably degraded. To confirm this, we treated the FAZ2 RNAi cells with MG-132, an inhibitor of the 26S proteasome. Cells induced for 72 h were chosen because, at this time point, the RNAi cells were still alive and had the lowest level of FAZ1. The results showed that FAZ1 was stabilized in the cytosolic fraction, albeit there was also a slight increase in FAZ1 level in the cytoskeletal fraction (Fig. 2C). These results suggest that upon FAZ2 depletion, the majority of FAZ1 accumulated in the cytosol, where it was subsequently degraded.

To test whether the effect of FAZ2 RNAi on FAZ1 stability is specific, we examined another FAZ filament protein, Tb927.7.3330 (Morriswood et al., 2013). Immunofluorescence microscopy showed that endogenously 3HA-tagged Tb927.7.3330 was detected at the short new FAZ filament and the old FAZ filament in FAZ2 RNAi cells (Fig. 2D), similar to FAZ1 (Fig. 2A). Western blotting showed that the Tb927.7.3330 level started to decrease after FAZ2 RNAi for 24 h and was decreased to ~30% of the control level after 72 h (Fig. 2E). When MG-132 was added to the RNAi cells, Tb927.7.3330 was stabilized (Fig. 2F), suggesting that this protein was also degraded upon FAZ2 RNAi.

Identification of new FAZ filament proteins by 2D-DiGE

The effect of FAZ2 RNAi on FAZ1 and Tb927.7.3330 stability suggests that FAZ2 depletion could exert a similar effect on other FAZ filament proteins, which, in turn, would allow us to identify

Journal of Cell Science (2015) 128, 2361-2372 doi:10.1242/jcs.168377

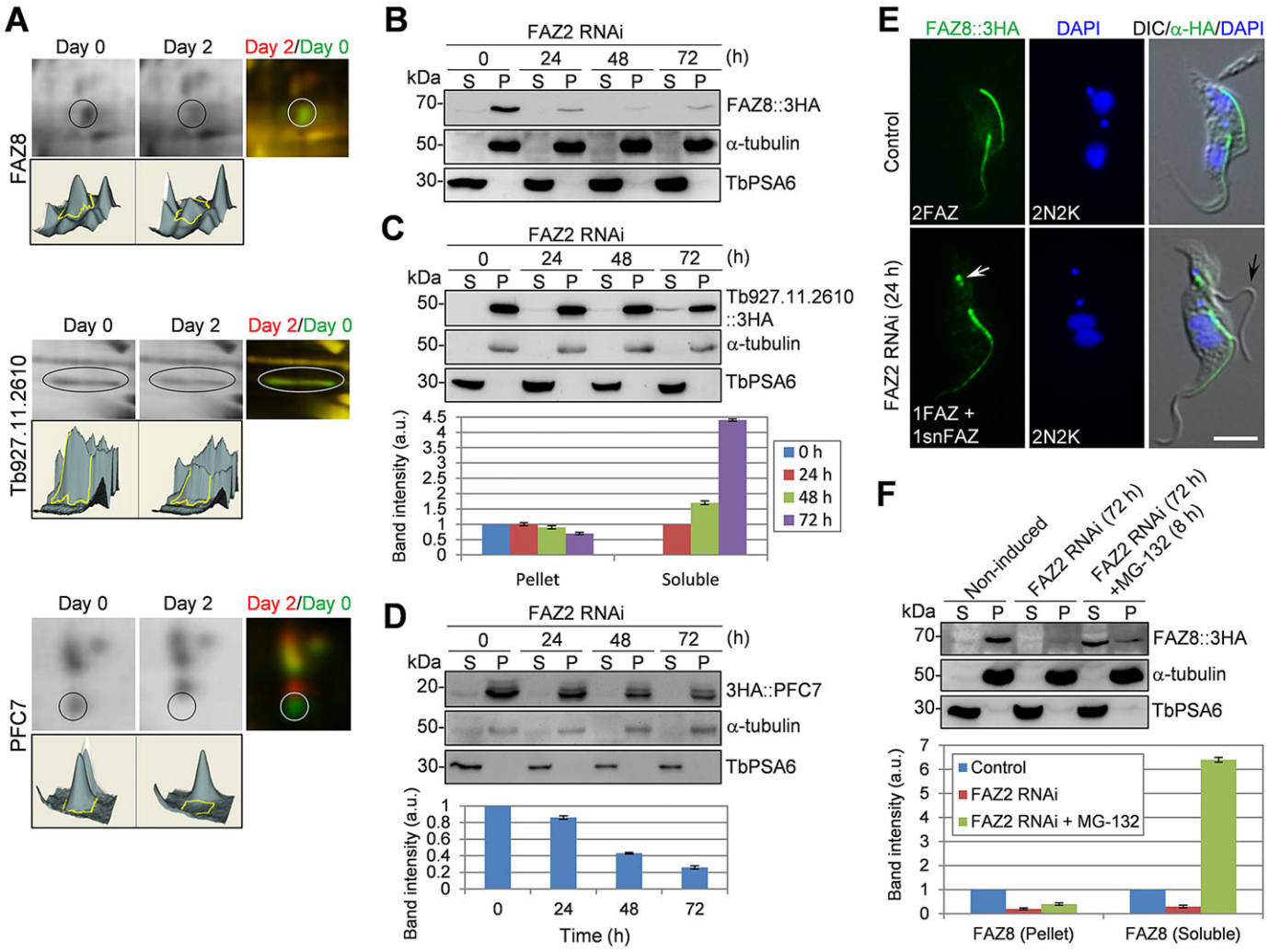

Fig. 3. Identification of proteins down-regulated upon FAZ2 RNAi. (A) Two-dimensional DiGE analysis of FAZ2 RNAi non-induced and induced cytoskeletons. Shown are the 2D images of three representative proteins, FAZ8, Tb927.11.2610 and PFC7, in non-induced and FAZ2 RNAi induced cells. The 2D gel was analyzed using DeCyder software to generate three-dimensional images of the three protein spots that show a reduction in volume after FAZ2 RNAi induction. (B–D) Levels of FAZ8, Tb927.11.2610 and PFC7 in FAZ2 RNAi cells. FAZ8 (B), Tb927.11.2610 (C) and PFC7 (D) were each endogenously tagged with a triple HA epitope in FAZ2 RNAi cells. The three proteins were detected with anti-HA antibody. α-tubulin and TbPSA6 were included as cytoskeletal and cytosolic markers, respectively. Protein band intensity was determined as described in Fig. 2, and plotted as histograms, shown below the western blots. Error bars indicate s.d. calculated from three independent experiments. (E) Immunostaining of 3HA-tagged FAZ8 in control and FAZ2 RNAi cells. White arrows indicate the short new FAZ filament (snFAZ) associated with the detached new flagellum (black arrows). Scale bar: 5 µm. (F). Stability of 3HA-tagged FAZ8 in non-induced control and FAZ2 RNAi cells. FAZ2 RNAi was induced with tetracycline for 72 h or with tetracycline for 72 h and MG-132 for 8 h. Immunoblotting was carried out with anti-HA mAb. The same blot was re-probed with anti-α-tubulin and anti-TbPSA6. Protein band intensity was determined as described in Fig. 2, and plotted as a histogram, shown below the western blots. Error bars represent s.d. calculated from three independent experiments. S, cytosolic fraction; P, cytoskeletal fraction.

new FAZ filament proteins by a comparative proteomic approach. To this end, we prepared cytoskeletons of non-induced control cells and FAZ2 RNAi cells induced for 1 and 2 days for two-dimensional difference gel electrophoresis (2D-DiGE) analysis (Fig. 3A; supplementary material Fig. S1). We focused on those proteins whose levels were reduced upon FAZ2 RNAi for both time points, and based on this criterion we selected 20 protein spots for mass spectrometry. A total of 14 out of the 20 proteins thus identified have been reported to associate with the flagellum, eight of which were previously found in the flagellum proteome and are of unknown function (Broadhead et al., 2006) and six of which were previously identified as components of the PFR (Portman et al., 2009) (supplementary material Table S1). Given that we aimed to identify new FAZ filament proteins, only the eight flagellum-associated hypothetical proteins were further characterized. Each of the eight proteins was tagged with a triple HA epitope and expressed from their respective endogenous locus, and immunofluorescence microscopy showed distinct localizations (supplementary material Fig. S2). One protein (Tb927.4.2060) was localized to the FAZ filament and was named FAZ8, one protein (Tb927.8.6230) was localized to the flagellum, two proteins were localized to both the flagellum and the cytoplasm, one protein was localized to both the flagellum and the cytoskeleton, and three proteins were localized to the cytoskeleton (supplementary material Fig. S2). Based on the localizations of the eight proteins and previous work on the six PFR proteins (Portman et al., 2009), the 14 proteins that were down-regulated in FAZ2 RNAi cells were assigned to one of six distinct groups: FAZ protein, flagellum protein, flagellum and cytoplasm protein, flagellum and cytoskeleton protein, cytoskeleton protein, or PFR

Journal of Cell Science (2015) 128, 2361-2372 doi:10.1242/jcs.168377

protein (supplementary material Table S1). None of the known FAZ filament proteins, including FAZ2 itself, were among the 20 protein spots selected for mass spectrometry. It should be noted that many protein spots on the 2D gel (supplementary material Fig. S2) that showed decreased levels after FAZ2 RNAi were not selected for mass spectrometry due to budget constraint. FAZ2 and other known FAZ proteins might be among those unselected protein spots. Nevertheless, this experiment still enabled us to identify FAZ8. Moreover, it also showed that some PFR components and some flagellum and cytoskeleton proteins were affected by FAZ2 depletion (Fig. 3; supplementary material Table S1), which further confirmed that flagellum adhesion might involve proteins from the FAZ filament, the PFR and the cytoskeleton (Ginger et al., 2013; Rotureau et al., 2014; Sun et al., 2013).

To confirm that these proteins were indeed affected by FAZ2 RNAi, we chose three proteins from three different groups, FAZ8, as a FAZ filament protein, Tb927.11.2610, as a representative of the cytoskeletal proteins, and PFC7 as a representative of the PFR proteins, for further characterization. Each of the three proteins was tagged with a triple HA epitope and expressed from their respective endogenous locus in FAZ2 RNAi cell line. Cells induced for FAZ2 RNAi for different times were assayed by western blot to detect the levels of the three proteins in cytosolic and cytoskeletal fractions. In non-induced control cells, all three proteins were mainly detected in the cytoskeletal fraction (Fig. 3B–D). The FAZ8 level started to decrease after FAZ2 RNAi for 24 h (Fig. 3B). Tb927.11.2610 level was also gradually decreased, but was only slightly (~30%) reduced after FAZ2 RNAi for 72 h (Fig. 3C). Interestingly, the level of Tb927.11.2610 in the cytosolic fraction appeared to be slightly increased (Fig. 3C), suggesting that a small amount of Tb927.11.2610 accumulated in the cytosol upon FAZ2 RNAi. Unlike FAZ8 and Tb927.11.2610, PFC7 was moderately affected, with its level decreased to ~25% of the control level after FAZ2 RNAi for 72 h (Fig. 3D).

Immunofluorescence microscopy further showed that FAZ8 was present at the short new FAZ filament and the old FAZ filament in FAZ2 RNAi cells (Fig. 3E). To examine whether FAZ8 was degraded upon FAZ2 RNAi, MG-132 was added to FAZ2 RNAi cells, and western blotting showed that FAZ8 was stabilized (Fig. 3F). This result suggests that FAZ8 was indeed degraded upon FAZ2 RNAi.

FAZ2 forms a complex with CC2D and KMP11

To identify potential FAZ2 partner(s), we expressed FAZ2 tagged with a C-terminal Protein-A–TEV–Protein-C (PTP) epitope (Schimanski et al., 2005) from one of its endogenous loci and carried out immunoprecipitation. To solubilize FAZ2 and its potential interacting partner(s) from the FAZ filament, cells were treated with high salt (500 mM NaCl) and lysed by thorough sonication prior to immunoprecipitation. The immunoprecipitate was eluted with Rapigest, digested with trypsin and analyzed by liquid-chromatography tandem mass spectrometry (LC-MS/MS). Peptides of three proteins, FAZ2, CC2D (Zhou et al., 2011) and KMP11 (Li and Wang, 2008), were highly enriched in the immunoprecipitate (supplementary material Table S2), suggesting that CC2D and KMP11 could be FAZ2 partners. To confirm their *in vivo* interactions, co-immunoprecipitation was performed, which showed that immunoprecipitation of FAZ2–PTP and KMP11–PTP both pulled down CC2D (Fig. 4A,B) and immunoprecipitation of KMP11–PTP precipitated FAZ2–3HA (Fig. 4C). These results suggest that FAZ2, CC2D and KMP11 form a complex *in vivo*.

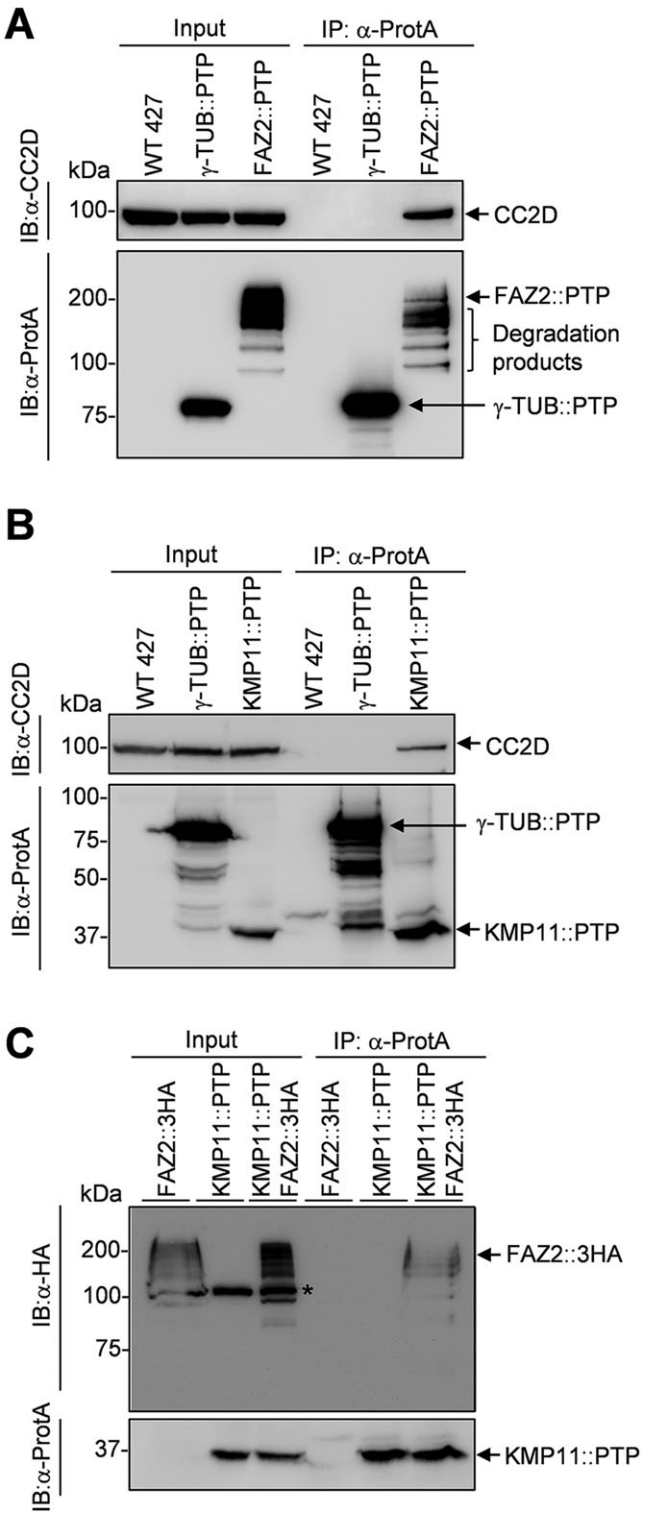

Fig. 4. FAZ2 forms a complex with CC2D and KMP11. (A,B) Co-immunoprecipitation of CC2D by FAZ2 (A) and KMP11 (B). FAZ2–PTP and KMP11–PTP were precipitated by incubating with IgG sepharose beads, and the immunoprecipitate (IP) was immunoblotted with anti-CC2D and anti-Protein A (α-ProtA) to detect CC2D and PTP-tagged FAZ2 and KMP11, respectively. PTP-tagged γ-tubulin (γ-TUB::PTP) was included as a negative control. (C) Co-immunoprecipitation of FAZ2–3HA (FAZ2::3HA) by KMP11–PTP (KMP11::PTP). FAZ8–3HA and KMP11–PTP were co-expressed from their respective endogenous locus in the same cell line. Cells expressing FAZ2–3HA or KMP11–PTP served as controls. The asterisk shows a non-specific band detected by anti-HA antibody in the input, but not in the immunoprecipitates.

Journal of Cell Science (2015) 128, 2361-2372 doi:10.1242/jcs.168377

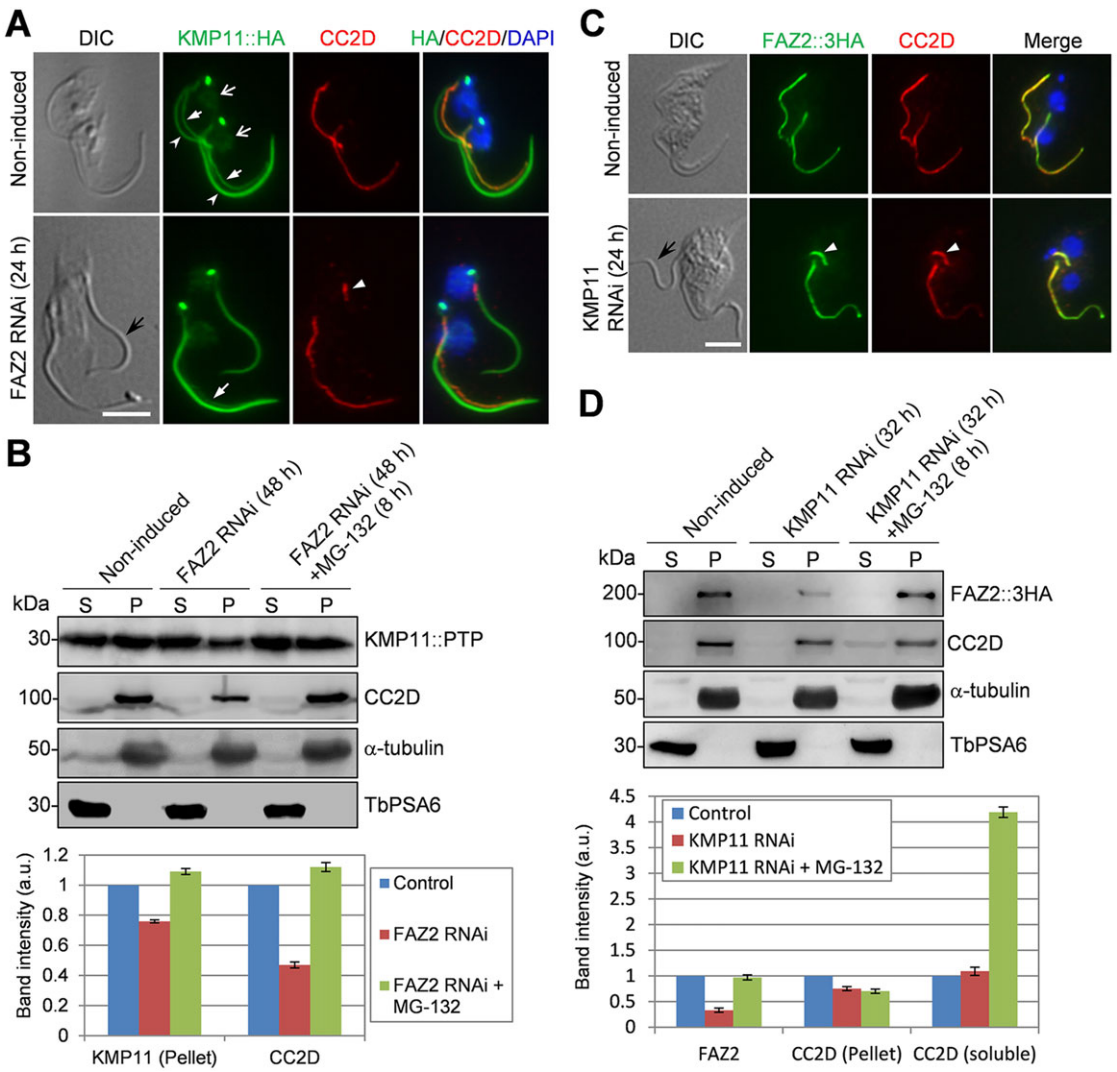

Fig. 5. FAZ2 RNAi destabilizes CC2D and KMP11, and KMP11 RNAi destabilizes FAZ2 and CC2D. (A) The effect of FAZ2 depletion on CC2D and KMP11 localization. KMP11 was endogenously tagged in FAZ2 RNAi cells. Cells were co-immunostained with FITC-conjugated anti-HA mAb and anti-CC2D pAb. Solid white arrows indicate KMP11 signal in the FAZ filaments, open white arrows indicate KMP11 signal in the nuclei, open arrowheads indicate KMP11 signal in the flagella, and the white arrowhead shows CC2D signal at the proximal base of the detached new flagellum (black arrow). The two bright green fluorescence dots at the proximal base of the flagella are KMP11 signal in the basal bodies. Scale bar: 5 µm. (B) Stability of CC2D and KMP11 in FAZ2 RNAi cells. FAZ2 RNAi cell line expressing endogenously PTP-tagged KMP11 was induced with tetracycline for 72 h or with tetracycline for 72 h and MG-132 for 8 h. Soluble and pellet fractions were immunoblotted with anti-CC2D and anti-Protein A to detect CC2D and KMP11–PTP (KMP11::PTP), respectively. The same membrane was re-blotted with anti-α-tubulin and anti-TbPSA6. Protein band intensity was determined as described in Fig. 2, and plotted as a histogram, shown below the western blots. Error bars represent s.d. calculated from three independent experiments. S, cytosolic fraction; P, cytoskeleton fraction. (C) Effect of KMP11 RNAi on FAZ2 and CC2D localization. FAZ2 was endogenously tagged with a triple HA epitope in KMP11 RNAi cell line. Cells were co-immunostained with a FITC-conjugated anti-HA mAb and anti-CC2D pAb. White arrowheads show FAZ2–3HA (FAZ2::3HA) and CC2D in the proximal base of the detached new flagellum (black arrow). Scale bar: 5 µm. (D). Stability of FAZ2 and CC2D in KMP11 RNAi cells. KMP11 RNAi cell line expressing FAZ2–3HA was induced with tetracycline for 32 h or with tetracycline for 32 h and MG-132 for 8 h. Soluble and pellet fractions were immunoblotted with anti-CC2D pAb and anti-HA mAb to detect CC2D and FAZ2–3HA, respectively. The same membrane was re-blotted with anti-α-tubulin and anti-TbPSA6 as cytoskeletal and cytosolic markers, respectively. Protein band intensity was determined as described in Fig. 2, and is plotted as a histogram shown below the western blots. Error bars indicate s.d. calculated from three independent experiments. S, cytosolic fraction; P, cytoskeletal fraction.

Interdependence of FAZ2, CC2D and KMP11 for protein stability

The identification of KMP11 as a FAZ2 partner is unexpected because KMP11 has been previously shown to localize to the flagella and the basal body even though RNAi against KMP11 has been shown to disrupt the new FAZ filament (Li and Wang, 2008). In that previous report, localization of KMP11 was determined using paraformaldehyde-fixed intact cells, which might not be able to allow the KMP11 fluorescence signal in the FAZ filament to be distinguished from that in the flagellum if KMP11 also localizes to the FAZ filament. To test whether KMP11 additionally localizes to the FAZ filament, we prepared detergent-extracted cytoskeletons in which the FAZ filament and the flagellum are visually separated. Immunofluorescence microscopy showed that endogenously HA-tagged KMP11 was indeed localized to the FAZ filament (Fig. 5A, solid white arrows), as shown by co-localization with CC2D, in addition to the flagellum and the basal body (Fig. 5A). Moreover, KMP11–HA was also detected in the nucleus (Fig. 5A, open white arrows), which is consistent with its previously reported role in mitosis (Li and Wang, 2008).

Journal of Cell Science (2015) 128, 2361-2372 doi:10.1242/jcs.168377

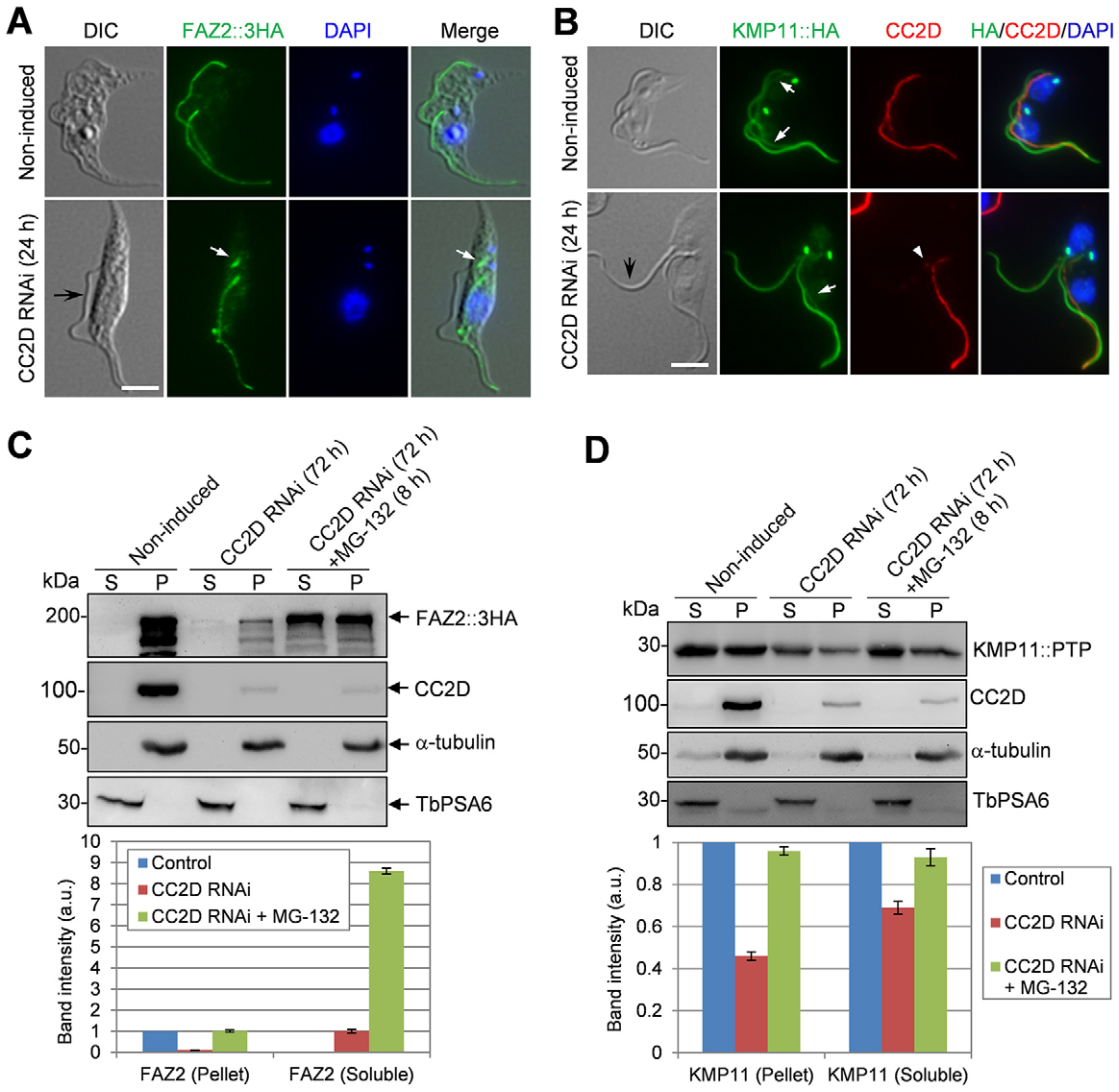

Fig. 6. CC2D depletion destabilizes FAZ2 and KMP11. (A) Effect of CC2D RNAi on the localization of FAZ2. FAZ2 was endogenously tagged with a C-terminal triple HA epitope in cells harboring a CC2D RNAi construct. Cells were immunostained with FITC-conjugated anti-HA mAb. The white arrow shows FAZ2–3HA (FAZ2::3HA) at the proximal base of detached new flagellum, and the black arrow indicates the detached new flagellum. Scale bar: 5 µm. (B) Effect of CC2D RNAi on KMP11 localization. KMP11 was endogenously tagged with an HA tag in CC2D RNAi cell line. Cells were co-immunostained with FITC-conjugated anti-HA mAb and anti-CC2D pAb. White arrows indicate the KMP11–HA (KMP11::HA) in the FAZ filament, whereas the white arrowhead shows the CC2D signal at the proximal base of the detached new flagellum (black arrow). Scale bar: 5 µm. (C,D) Stability of FAZ2 (C) and KMP11 (D) in CC2D RNAi cells. CC2D RNAi cell line expressing endogenously 3HA-tagged FAZ2 or PTP-tagged KMP11 was induced with tetracycline for 72 h or with tetracycline for 72 h and MG-132 for 8 h. Soluble and pellet fractions were immunoblotted with anti-HA mAb and anti-CC2D pAb to detect FAZ2–3HA and CC2D, respectively, or with anti-Protein A antibody and anti-CC2D antibody to detect KMP11–PTP and CC2D, respectively. The same membrane was re-blotted with anti-α-tubulin and anti-TbPSA6. Protein band intensity was determined as described in Fig. 2, and plotted as histograms, shown below the western blots. Error bars indicate s.d. calculated from three independent experiments. S, cytosolic fraction; P, cytoskeletal fraction.

Given that FAZ2 forms a complex with CC2D and KMP11, we examined the effect of FAZ2 depletion on the localization and stability of CC2D and KMP11. Upon FAZ2 RNAi, CC2D was detected at the short new FAZ filament and the old FAZ filament (Fig. 5A), but endogenously HA-tagged KMP11 was not readily detectable at the short new FAZ filament (Fig. 5A). We then examined the levels of CC2D and KMP11 in FAZ2 RNAi cells. Western blotting showed that the levels of CC2D and endogenously PTP-tagged KMP11 in the cytoskeletal fraction were decreased to ~50% and ~75% of the control level, respectively (Fig. 5B). The KMP11 level in the cytosolic fraction, however, appeared to be unchanged (Fig. 5B). In the presence of MG-132, CC2D and KMP11 in the cytoskeletal fraction were stabilized (Fig. 5B). These results suggest that FAZ2 depletion partially destabilized CC2D and KMP11. The partial de-stabilization of KMP11 by FAZ2 RNAi could be attributed to the fact that KMP11 localizes to multiple structures and that only FAZ-filament-localizing KMP11 was affected by FAZ2 RNAi.

Similar to the effect of FAZ2 depletion on the stability of CC2D and KMP11, KMP11 RNAi impaired the stability of FAZ2 and CC2D (Fig. 5C,D), and CC2D RNAi destabilized FAZ2 and KMP11 (Fig. 6).

FAZ filament proteins are incorporated into the FAZ filament from the proximal region

The presence of a short new FAZ filament upon FAZ2 RNAi (Fig. 2) suggests that FAZ filament proteins are probably assembled from the proximal base of the new FAZ filament during the biogenesis of the

Journal of Cell Science (2015) 128, 2361-2372 doi:10.1242/jcs.168377

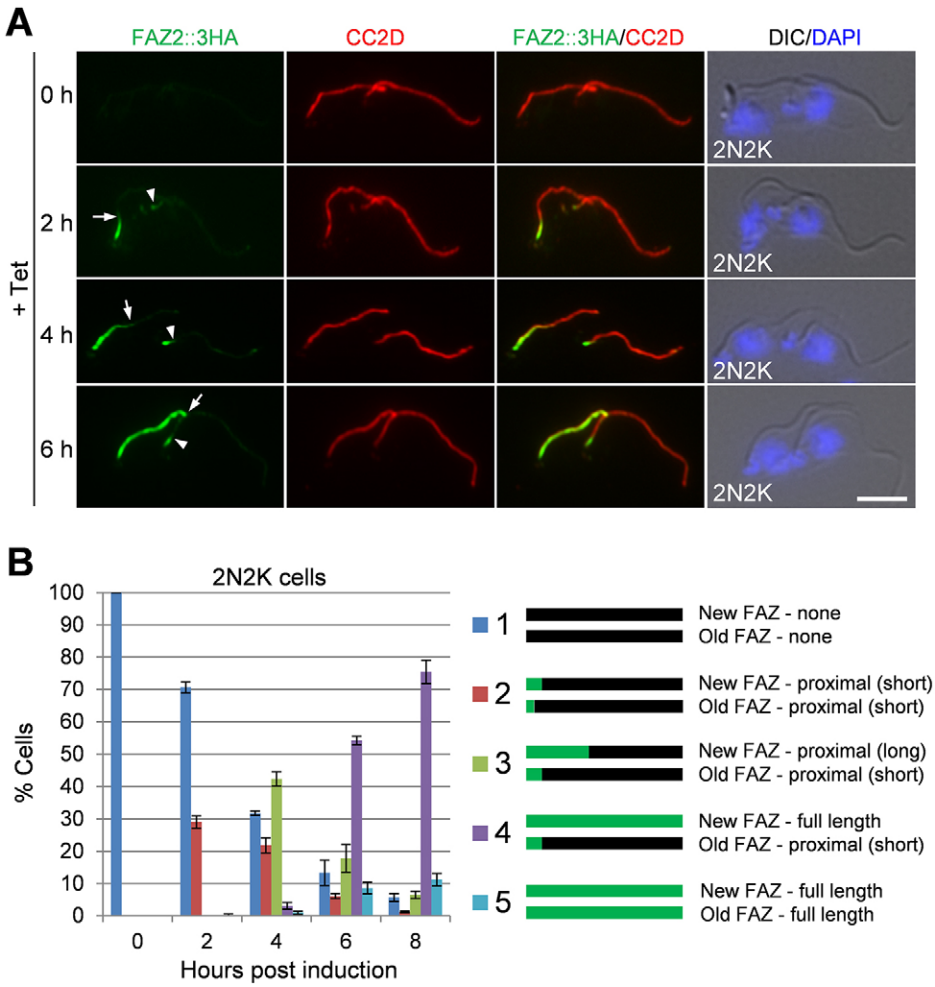

Fig. 7. FAZ2 is incorporated into the FAZ filament from the proximal region. (A) Incorporation of FAZ2–3HA (FAZ2::3HA) into the FAZ filament examined by immunofluorescence microscopy. Cells induced with 1.0 µg/ml tetracycline for various times (h) were co-immunostained with FITC-conjugated anti-HA mAb and anti-CC2D pAb. Arrows and arrowheads indicate the growing tips of the FAZ2–3HA fluorescence signal in the new and old FAZ filaments, respectively. Scale bar: 5 µm. (B) Quantification of 2N2K cells with different types of FAZ2–3HA pattern in the new and old FAZ filaments. ~200 cells were counted, and error bars represent s.d. calculated from three independent experiments.

new FAZ filament. To test this possibility, we ectopically overexpressed a triple HA-tagged FAZ2 in a tetracycline-inducible manner and carried out a time-course experiment to monitor the incorporation of FAZ2–3HA into the FAZ filament by fluorescence microscopy (Fig. 7A). A clonal cell line induced with tetracycline for different times was co-immunostained with anti-HA antibody, to detect FAZ2–3HA, and anti-CC2D antibody to label the existing FAZ filament, and the 2N2K cells with different types of FAZ2–3HA patterns were counted. We did not count 1N2K cells because the new FAZ filament in these cells had various lengths, making it difficult to distinguish between the elongating FAZ2–3HA signal and the full-length FAZ2–3HA signal. After 2 h of induction, FAZ2–3HA was clearly detectable at the proximal base of the new FAZ filament (Fig. 7A, 2 h, arrow; Fig. 7B). After induction for 4 h, FAZ2–3HA fluorescence signal at the new FAZ filament gradually elongated towards the distal tip (Fig. 7A, 4 h, arrow; Fig. 7B). After induction for 6 h, the FAZ2–3HA signal reached the distal tip of the new FAZ (Fig. 7A, 6 h, arrow; Fig. 7B). However, FAZ2–3HA in the old FAZ filament was first detected at 2 h but had not substantially extended after induction for 6 h (Fig. 7A, arrowheads) or even 8 h (Fig. 7B) in the majority (~90%) of the 2N2K cells examined. We found that lower or higher levels of FAZ2–3HA induced with lower or higher concentrations of tetracycline produced almost identical results (data not shown). Moreover, similar patterns of FAZ8 incorporation were also observed (supplementary material Fig. S3), suggesting that FAZ filament proteins might follow the same direction of incorporation.

Given that KMP11 localizes to the flagellum and the FAZ filament, we ectopically overexpressed KMP11 so that we could examine its incorporation into the flagellum and the FAZ simultaneously. At 2 h post induction, KMP11–3HA was detected at the proximal base of the new FAZ filament (Fig. 8A, arrows). Subsequently, the signal was gradually extended to the distal tip of the new FAZ filament (Fig. 8A, arrows), similar to the pattern of FAZ2–3HA and FAZ8–3HA incorporation. In the flagellum, however, KMP11–3HA was detected in the distal end of the new flagellum at 2 h of induction (Fig. 8A, arrowhead; Fig. 8B) and then was gradually extended towards the proximal region of the new flagellum after induction for longer times (Fig. 8A, arrowheads; Fig. 8B), suggesting that KMP11 in the flagellum was incorporated from the distal end of the flagellum. Using a similar overexpression approach, the PFR component PFR2 (Bastin et al., 1999) was also found to be incorporated from the distal tip of the flagellum. Taken together, these results suggest that the FAZ filament components are incorporated into the new FAZ filament from the proximal region. This appears to be opposite to the direction of incorporation of flagellum components, which are incorporated into the new flagellum from the distal end (Fig. 8C).

DISCUSSION

Although the roles of the FAZ filament in maintaining flagellum adhesion and defining the cytokinesis cleavage plane are well understood, our knowledge about the composition and assembly of the FAZ filament is still very limited. To date, as many as nine

Journal of Cell Science (2015) 128, 2361-2372 doi:10.1242/jcs.168377

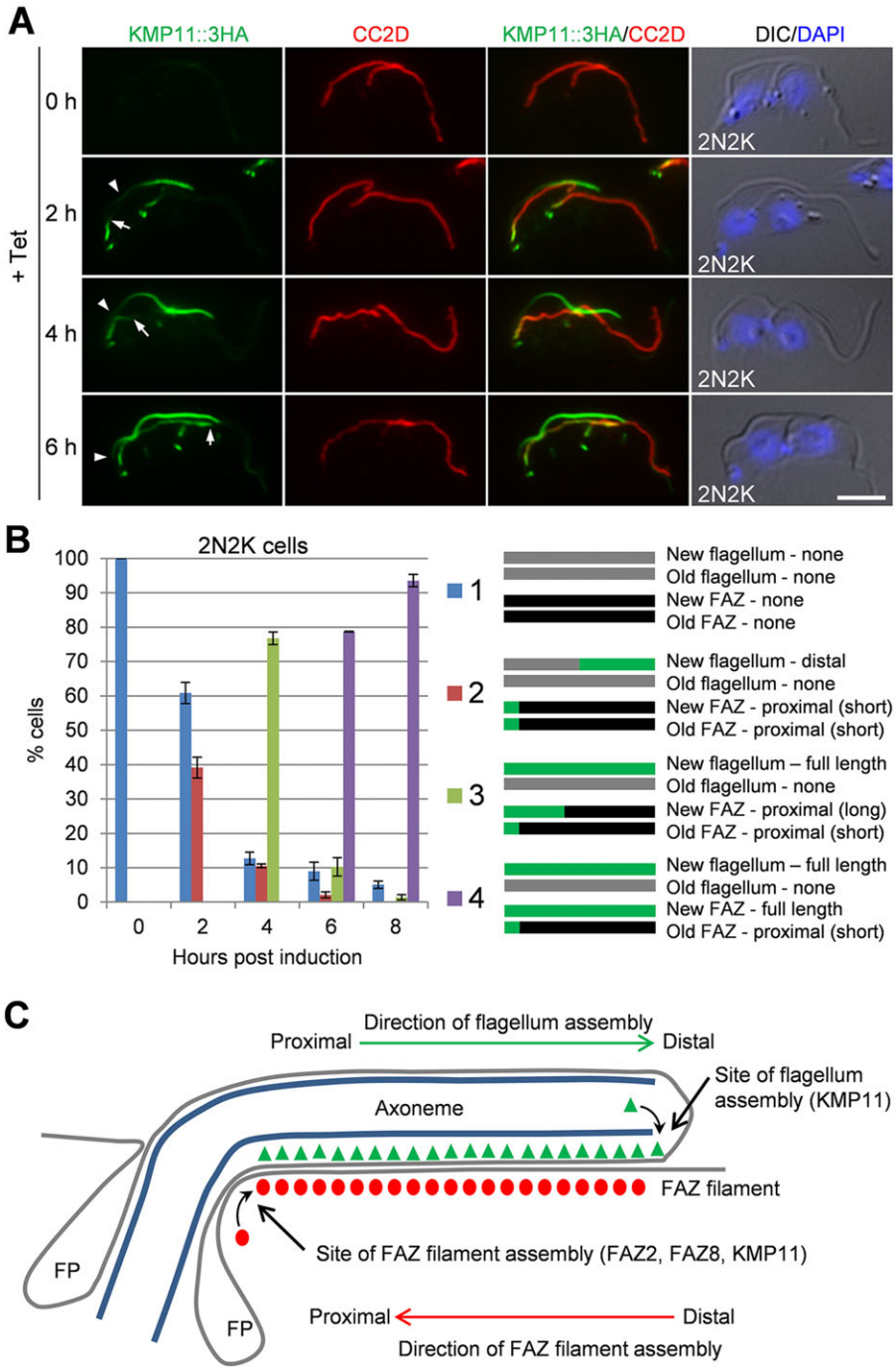

Fig. 8. KMP11 is incorporated into the FAZ filament from the proximal region and into the flagellum from the distal region. (A) Incorporation of KMP11–3HA (KMP11::3HA) into the FAZ filament and the flagellum examined by immunofluorescence microscopy. Arrows and arrowheads indicate the growing tips of KMP11–3HA in the FAZ filament and the flagellum, respectively. Scale bar: 5 µm. (B). Quantification of 2N2K cells with different types of KMP11–3HA pattern in the new and old FAZ filaments and in the new and old flagella. ~200 cells were counted, and error bars represent s.d. calculated from three independent experiments. (C). Model of the assembly of the FAZ filament proteins and the flagellum component in procyclic trypanosomes, showing the proximal assembly of the FAZ filament proteins (FAZ2, FAZ8 and KMP11) and the distal assembly of flagellum component (KMP11). FP, flagellar pocket.

proteins, four of which contain trans-membrane domains, have been localized to the FAZ filament, suggesting that the composition of the FAZ filament is complex. In this report, we added three new proteins, FAZ2, FAZ8 and KMP11, to the list of FAZ filament proteins. FAZ2 was identified by screening known flagellum-associated proteins for those that located to the FAZ filament (Zhou et al., 2010), FAZ8 was discovered by a comparative proteomic approach to search for proteins downregulated upon FAZ2 depletion (Fig. 3), and KMP11 was identified as a FAZ2 partner (Fig. 4). Both FAZ2 and FAZ8 contain a number of coiled coil motifs but lack any predicted trans-membrane domain, suggesting that they might function as structural components of the FAZ filament. Although FAZ2 is essential for cell viability (Fig. 1), RNAi against FAZ8 in the procyclic form did not cause any growth defect (data not shown), suggesting that either FAZ8 is dispensable in the procyclic form or RNAi of FAZ8 is insufficient to reveal any defects. Previous genome-wide RNAi screens have shown that FAZ8 is not essential in the procyclic form, but that depletion causes a growth defect in the bloodstream form (Alsford et al., 2011). The function of FAZ8 in the bloodstream form remains to be explored.

Through immunoprecipitation, we identified a FAZ filament protein complex formed by FAZ2, CC2D and KMP11 (Fig. 4; supplementary material Table S2). RNAi against each of the three proteins resulted in full detachment of the new flagellum (Figs 2, 5 and 6), which differs from the FAZ1 RNAi phenotype, which only shows partial flagellum detachment (Vaughan et al., 2008). This suggests

Journal of Cell Science (2015) 128, 2361-2372 doi:10.1242/jcs.168377

that different FAZ proteins play distinct roles in FAZ filament assembly and flagellum adhesion. However, it should be noted that CC2D is additionally localized to basal body (Zhou et al., 2011) and KMP11 is additionally localized to basal body, flagellum and nucleus (Fig. 5), suggesting that CC2D and KMP11 have additional roles, whereas FAZ2 is probably only involved in FAZ filament assembly.

FAZ2 depletion appeared to exert profound effects on the cytoskeletal structures along the FAZ filament by affecting the stability of multiple FAZ filament proteins and several cytoskeleton and flagellum proteins (Figs 2 and 3; supplementary material Table S1). This finding suggests that flagellum adhesion involves proteins from the FAZ filament, the flagellum and the cytoskeleton. Although the requirement for FAZ proteins in flagellum adhesion has been well established (Oberholzer et al., 2011; Vaughan et al., 2008; Woods et al., 2013; Zhou et al., 2011), the involvement of flagellum proteins, especially the PFR proteins, in flagellum adhesion has also been recently demonstrated (Ginger et al., 2013; Rotureau et al., 2014). Our finding that FAZ2 depletion affected six PFR proteins (supplementary material Table S1; Fig. 3) suggests the involvement of additional PFR proteins in flagellum adhesion. However, it should be noted that these PFR proteins were only moderately affected upon FAZ2 RNAi (Fig. 3D; supplementary material Fig. S1), which did not disrupt the overall structure of the PFR (data not shown). Unlike the PFR protein and the cytoskeleton protein (Fig. 3C,D), however, the FAZ proteins were more drastically affected (Fig. 2; Fig. 3B). It appears that when FAZ2 was depleted, other FAZ filament proteins investigated in this study, whether they interact with FAZ2 or not, were all destabilized. This interesting finding means that it is tempting to suggest that it is the defective assembly of the new FAZ filament, rather than the depletion of individual FAZ filament proteins per se, that caused the destabilization of FAZ filament proteins. In this regard, proper assembly of the FAZ filament appears to be necessary to maintain the stability of FAZ filament proteins.

Our result also demonstrated that FAZ filament proteins are incorporated into the new FAZ filament from the proximal region near the flagellar pockect. This conclusion is supported by the fact that ectopically overexpressed FAZ2, FAZ8 and KMP11 were all first incorporated into the proximal region of the new FAZ filament (Figs 7, 8; supplementary material Fig. S3). This pattern of incorporation is opposite to that of the flagellum components, such as KMP11 (Fig. 8) and PFR2 (Bastin et al., 1999), which are incorporated from the distal tip of the new flagellum. While this article was in revision, Sunter and colleagues reported the identification of eight new FAZ proteins by proteomics and bioinformatics (Sunter et al., 2015), which also include the FAZ2 and FAZ8 proteins identified in this work. By overexpressing eYFP-tagged FAZ proteins, they also found that FAZ filament proteins were incorporated into the FAZ filament from the proximal region, which is in contrast to the incorporation of PFR2 into the flagellum (Sunter et al., 2015). Our results therefore provide independent evidence to support the view that the FAZ filament and the flagellum have distinct assembly sites, that is, at the proximal region and at the distal end, respectively (Fig. 8C). In *T. brucei*, assembly of the new flagellum and its FAZ filament must be well coordinated. Although they both originate from the proximal base and extend to the anterior tip, components of the flagellum and the FAZ filament appear to be incorporated in opposite directions during their biogenesis. It remains unclear how trypanosome cells coordinate the elongation of the new flagellum and its FAZ filament to ensure proper cell morphogenesis.

Assembly of the new FAZ filament appears to be initiated from the bilobe region (Esson et al., 2012) by initially forming a short FAZ root around the bilobe, which likely represents the initial FAZ nucleation and is known to occur before, and independently of, the assembly of the new flagellum (Kohl et al., 2003, 1999). Through unknown mechanisms, this short FAZ root was maintained when FAZ filament proteins, such as FAZ2, CC2D or KMP11, were depleted (Figs 2, 3, 5 and 6) and when the flagellum protein FLAM3 was depleted (Rotureau et al., 2014). It is unclear whether the bilobe structure plays any role to help assemble this short FAZ root, but inhibition of bilobe formation by RNAi of TbLRRP1 completely abolishes the assembly of the new FAZ filament, including the short FAZ root (Zhou et al., 2010). Additionally, depletion of BIBLO-1, a flagellar pocket collar component, also completely disrupts the new FAZ filament and the short FAZ root (Bonhivers et al., 2008). Given the physical association between the fishhook of the bilobe structure and the flagellar pocket collar (Esson et al., 2012), it is unclear whether defective assembly of the flagellar pocket collar caused by BILBO-1 depletion disrupts bilobe duplication. Nevertheless, the involvement of bilobe and flagellar pocket collar in FAZ filament assembly might suggest that there is coordination between the assembly of the FAZ filament and the biogenesis of the bilobe and flagellar pocket collar.

MATERIALS AND METHODS

Trypanosome cell lines, RNAi and protein overexpression

The procyclic 427 cell line was cultured at 27°C in SDM-79 medium containing 10% fetal bovine serum (Atlanta Biologicals, Inc). The procyclic 29-13 cell line (Wirtz et al., 1999) was grown in the SDM-79 medium plus 10% fetal bovine serum, 15 µg/ml G418, and 50 µg/ml hygromycin.

For RNAi of FAZ2, CC2D and KMP11, DNA fragments (see supplementary material Table S3 for primer sequences) corresponding to the N-terminal coding region of *FAZ2* and *CC2D* and the full-length sequence of *KMP11* were each cloned into the pZJM vector. Transfection, generation of clonal cell lines, and RNAi were carried out according to our previously published procedures (Wei et al., 2014).

To overexpress 3HA-tagged FAZ2, FAZ8 and KMP11, the full-length CDS of the three genes were each cloned into pLew100-3HA vector, and the resulting constructs were transfected into 29-13 cell lines. Clonal cell lines were generated by limiting dilution in a 96-well plate by adding 20% fetal bovine serum to the medium. To induce the overexpression of these proteins, different concentrations of tetracycline (0.1 µg/ml, 0.5 µg/ml, and 1.0 µg/ml) were added into the cell culture to achieve different levels of overexpressed proteins.

In situ epitope tagging of proteins

For endogenous epitope tagging of proteins, DNA fragments corresponding to the C-terminal coding region of *FAZ2* and other genes were each cloned into the pC-3HA-PAC or pC-3HA-NEO or pC-PTP-PAC vectors, and a DNA fragment corresponding to the N-terminal coding region of *PFC7* was cloned into the pN-3HA-PAC vector. Transfection was carried out as described above. Transfectants were selected with 1.0 µg/ml puromycin or 40 µg/ml G418 and cloned by limiting dilution. Successful gene tagging was confirmed by PCR and subsequent sequencing of the PCR fragment as well as by western blotting with anti-HA antibody or anti-Protein A antibody (Sigma-Aldrich).

Immunoprecipitation of the FAZ2 complex and LC-MS/MS

For PTP tagging of FAZ2, a 653-bp fragment of *FAZ2* gene corresponding to the C-terminal coding region was cloned into the pC-PTP-NEO vector (Schimanski et al., 2005), and the resulting construct was linearized and electroporated into the 427 cell line. Successful transfectants were selected under 40 µg/ml G418 and cloned by limiting dilution. For immunoprecipitation of the FAZ2 complex, cells (~2.5×10^9 cells) were incubated in 10 ml immunoprecipitation buffer (25 mM Tris-HCl pH 7.6, 500 mM NaCl, 1 mM DTT, 1% NP-40, and protease inhibitor cocktail) and then sonicated thoroughly. The cell lysate was centrifuged at 12,000 ***g*** at 4°C

for 30 min, and the supernatant was incubated with 50 µl settled IgG sepharose 6 Fast Flow beads (GE Healthcare) at 4°C for 1 h. After a thorough wash with the immunoprecipitation buffer, beads were washed a further three times with the pre-elution buffer (50 mM Tris-HCl pH 8.3, 75 mM KCl, and 1 mM EGTA). Proteins bound to the beads were eluted by incubating with 60 µl elution buffer (0.1% Rapigest in 50 mM Tris-HCl pH 8.3) at room temperature for 25 min.

Processing of eluted proteins for mass spectrometry was carried out according to published procedure (Akiyoshi and Gull, 2014). Eluted proteins were analyzed on an LTQ Orbitrap XL (Thermo-Fisher Scientific) interfaced with an Eksigent nano-LC 2D plus ChipLC system (Eksigent Technologies, Dublin, CA) at the Proteomics Core Facility of the University of Texas Health Science Center at Houston.

Data analysis was performed according to our previous publication (Wei et al., 2014). Raw data files were searched against the *Trypanosoma brucei* database (version 4) using the Mascot search engine. The search conditions used peptide tolerance of 10 ppm and MS/MS tolerance of 0.8 Da with the enzyme trypsin and two missed cleavages.

Co-immunoprecipitation

For PTP tagging of KMP11 and γ-tubulin, an 855-bp fragment of the 5′-UTR and the coding sequence of *KMP11* and a 1280-bp fragment of γ-tubulin gene corresponding to the C-terminal coding region were each cloned into the pC-PTP-NEO vector (Schimanski et al., 2005). The resulting constructs were electroporated into the 427 cell line. The KMP11–PTP-expressing cell line was then transfected with pC-FAZ2::3HA-PAC. For co-immunoprecipitation, cells were washed with PBS, incubated in immunoprecipitation buffer and then sonicated thoroughly. Immunoprecipitation was carried out as described above. Immunoprecipitates were probed with anti-CC2D polyclonal antibody (pAb; 1:2000 dilution) (Zhou et al., 2011), anti-HA antibody (1:5000 dilution), to detect FAZ2–3HA, and anti-Protein A pAb (1:5000 dilution, Sigma-Aldrich) to detect PTP-tagged FAZ2, KMP11 and γ-tubulin.

Immunofluorescence microscopy

Cells were settled onto glass coverslips, fixed with cold methanol (−20°C), and then rehydrated with PBS. After blocking with 3% BSA in PBS for 1 h, coverslips were incubated with primary antibodies for 1 h at room temperature. The following primary antibodies were used: FITC-conjugated anti-HA monoclonal antibody (mAb; 1:400, Sigma-Aldrich), anti-CC2D pAb (1:1000 dilution) (Zhou et al., 2011) and L3B2 (anti-FAZ1 mAb, 1:50 dilution) (Kohl et al., 1999). After washing three times, coverslips were incubated with FITC- or Alexa-Fluor-594-conjugated secondary antibody for 1 h at room temperature. Slides were mounted with DAPI-containing VectaShield mounting medium (Vector Labs) and examined under an inverted fluorescence microscope (Olympus IX71) equipped with a cooled CCD camera (model Orca-ER, Hamamatsu) and a PlanApo N 60×1.42-NA DIC objective. Images were acquired using the Slidebook5 software (Intelligent Imaging Innovations).

Protein stability assay

Cells induced for FAZ2 or CC2D RNAi for 40 h or 64 h and for KMP11 RNAi for 32 h were split into two flasks. One was incubated with 1.0 µg/ml tetracycline, and the other was incubated with 1.0 µg/ml tetracycline and 50 µg/ml MG-132 (Selleckchem, Houston, TX) for an additional 8 h. Cells (10^7) were then lysed in 40 µl PEME buffer (100 mM PIPES pH 6.9, 2 mM EGTA, 0.1 mM EDTA, 1 mM $MgSO_4$) containing 1% NP-40, and centrifuged at 16,300 ***g*** for 10 min to separate cytosolic (soluble) and cytoskeletal (pellet) fractions. 40 µl of PEME buffer containing 1% NP-40 was then added to the pellet fraction. Subsequently, 10 µl of 5× SDS-PAGE sampling buffer was added to each of the two fractions and boiled. 20 µl of each sample was used for western blotting with anti-HA antibody, to detect 3HA-tagged proteins, or with anti-CC2D antibody. The same blots were then re-probed with anti-α-tubulin mAb (Sigma-Aldrich) and anti-TbPSA6 pAb, which recognizes the α6 subunit of the 26S proteasome (Li et al., 2002), as the cytoskeleton and cytosol markers, respectively. Protein band intensity was measured by ImageJ and normalized to that of the cytosolic and cytoskeletal loading controls, respectively. At least three independent experiments were carried out.

Two-dimensional DiGE

Non-induced control cells and FAZ2 RNAi-induced cells (2×10^8) were washed with PBS, treated with PEME buffer containing 1% NP-40 and protease inhibitor cocktail (Roche), and centrifuged at the highest speed (16,300 ***g***) in a microcentrifuge for 10 min at 4°C. The cytoskeleton was then lysed in 2-D cell lysis buffer (30 mM Tris-HCl pH 8.8, containing 7 M urea, 2 M thiourea and 4% CHAPS) by sonication on ice. The lysate was centrifuged at 11,000 ***g*** for 30 min at 4°C.

CyDye labeling and 2D-DiGE were carried out at Applied Biomics, Inc. Images were scanned immediately after SDS-PAGE using Typhoon TRIO (GE Healthcare) according to the manufacturer's instruction. The scanned images were analyzed by Image QuantTL software (GE Healthcare), and subject to in-gel analysis and cross-gel analysis using DeCyder software version 6.5 (GE Healthcare). The ratio change in protein levels was obtained from in-gel DeCyder software analysis.

Trypsin digestion, mass spectrometry and database search

The protein spots on the 2D gel were picked up by Ettan Spot Picker (GE Healthcare) based on the in-gel analysis and spot picking design by DeCyder software. The gel spots were washed a few times with water and digested in-gel with modified porcine trypsin protease (Trypsin Gold, Promega). The digested tryptic peptides were desalted by using a Zip-tip C18 (Millipore). Peptides were then eluted from the Zip-tip with 0.5 µl of matrix solution (a-cyano-4-hydroxycinnamic acid, 5 mg/ml in 50% acetonitrile, 0.1% trifluoroacetic acid, 25 mM ammonium bicarbonate) and spotted on the matrix-assisted laser desorption ionization (MALDI) plate.

MALDI-TOF (MS) and time-of-flight (TOF/TOF; tandem MS/MS) were performed on a 5800 mass spectrometer (AB Sciex). MALDI-TOF mass spectra were acquired in reflectron positive ion mode, averaging 2000 laser shots per spectrum. TOF/TOF tandem MS fragmentation spectra were acquired for each sample, averaging 2000 laser shots per fragmentation spectrum on each of the 10 most abundant ions present in each sample (excluding trypsin autolytic peptides and other known background ions).

Both the resulting peptide mass and the associated fragmentation spectra were submitted to GPS Explorer version 3.5 equipped with MASCOT search engine (Matrix science) to search the database of National Center for Biotechnology Information for non-redundant proteins (NCBInr). Searches were performed without constraining protein molecular mass or isoelectric point, with variable carbamidomethylation of cysteine and oxidation of methionine residues, and with one missed cleavage allowed in the search parameters. Candidates with either a protein score confidence interval percentage or ion confidence interval percentage greater than 95 were considered significant.

Acknowledgements

We thank Dr George A. M. Cross of Rockefeller University for providing the procyclic 29-13 cell line, Dr Paul T. Englund from Johns Hopkins University for the pZJM vector, Dr Arthur Günzl of University of Connecticut Health Center for the pC-PTP-NEO vector, and Dr Keith Gull of University of Oxford for L3B2 antibody.

Competing interests

The authors declare no competing or financial interests.

Author contributions

Q.Z. and Z.L. conceived and designed the experiments; Q.Z. and H.H. performed the experiments; Q.Z. and Z.L. analyzed the data; C.Y.H. contributed reagents, materials and analysis tools and edited the manuscript; Q.Z. and Z.L. wrote the manuscript.

Funding

This work was supported by the National Institutes of Health (NIH) [grant number R01AI101437 to Z.L.]. Deposited in PMC for release after 12 months.

Supplementary material

Supplementary material available online at
http://jcs.biologists.org/lookup/suppl/doi:10.1242/jcs.168377/-/DC1

References

Absalon, S., Kohl, L., Branche, C., Blisnick, T., Toutirais, G., Rusconi, F., Cosson, J., Bonhivers, M., Robinson, D. and Bastin, P. (2007). Basal body positioning is controlled by flagellum formation in *Trypanosoma brucei*. *PLoS ONE* **2**, e437.

Akiyoshi, B. and Gull, K. (2014). Discovery of unconventional kinetochores in kinetoplastids. *Cell* **156**, 1247-1258.
Alsford, S., Turner, D. J., Obado, S. O., Sanchez-Flores, A., Glover, L., Berriman, M., Hertz-Fowler, C. and Horn, D. (2011). High-throughput phenotyping using parallel sequencing of RNA interference targets in the African trypanosome. *Genome Res.* **21**, 915-924.
Bastin, P., MacRae, T. H., Francis, S. B., Matthews, K. R. and Gull, K. (1999). Flagellar morphogenesis: protein targeting and assembly in the paraflagellar rod of trypanosomes. *Mol. Cell. Biol.* **19**, 8191-8200.
Bonhivers, M., Nowacki, S., Landrein, N. and Robinson, D. R. (2008). Biogenesis of the trypanosome endo-exocytotic organelle is cytoskeleton mediated. *PLoS Biol.* **6**, e105.
Broadhead, R., Dawe, H. R., Farr, H., Griffiths, S., Hart, S. R., Portman, N., Shaw, M. K., Ginger, M. L., Gaskell, S. J., McKean, P. G. et al. (2006). Flagellar motility is required for the viability of the bloodstream trypanosome. *Nature* **440**, 224-227.
Esson, H. J., Morriswood, B., Yavuz, S., Vidilaseris, K., Dong, G. and Warren, G. (2012). Morphology of the trypanosome bilobe, a novel cytoskeletal structure. *Eukaryot. Cell* **11**, 761-772.
Ginger, M. L., Collingridge, P. W., Brown, R. W. B., Sproat, R., Shaw, M. K. and Gull, K. (2013). Calmodulin is required for paraflagellar rod assembly and flagellum-cell body attachment in trypanosomes. *Protist* **164**, 528-540.
Gull, K. (1999). The cytoskeleton of trypanosomatid parasites. *Annu. Rev. Microbiol.* **53**, 629-655.
Kohl, L., Sherwin, T. and Gull, K. (1999). Assembly of the paraflagellar rod and the flagellum attachment zone complex during the *Trypanosoma brucei* cell cycle. *J. Eukaryot. Microbiol.* **46**, 105-109.
Kohl, L., Robinson, D. and Bastin, P. (2003). Novel roles for the flagellum in cell morphogenesis and cytokinesis of trypanosomes. *EMBO J.* **22**, 5336-5346.
Lacomble, S., Vaughan, S., Deghelt, M., Moreira-Leite, F. F. and Gull, K. (2012). A *Trypanosoma brucei* protein required for maintenance of the flagellum attachment zone and flagellar pocket ER domains. *Protist* **163**, 602-615.
LaCount, D. J., Barrett, B. and Donelson, J. E. (2002). *Trypanosoma brucei* FLA1 is required for flagellum attachment and cytokinesis. *J. Biol. Chem.* **277**, 17580-17588.
Li, Z. and Wang, C. C. (2008). KMP-11, a basal body and flagellar protein, is required for cell division in *Trypanosoma brucei*. *Eukaryot. Cell* **7**, 1941-1950.
Li, Z., Zou, C.-B., Yao, Y., Hoyt, M. A., McDonough, S., Mackey, Z. B., Coffino, P. and Wang, C. C. (2002). An easily dissociated 26 S proteasome catalyzes an essential ubiquitin-mediated protein degradation pathway in *Trypanosoma brucei*. *J. Biol. Chem.* **277**, 15486-15498.
Morriswood, B., Havlicek, K., Demmel, L., Yavuz, S., Sealey-Cardona, M., Vidilaseris, K., Anrather, D., Kostan, J., Djinovic-Carugo, K., Roux, K. J. et al. (2013). Novel bilobe components in *Trypanosoma brucei* identified using proximity-dependent biotinylation. *Eukaryot. Cell* **12**, 356-367.
Oberholzer, M., Langousis, G., Nguyen, H. T., Saada, E. A., Shimogawa, M. M., Jonsson, Z. O., Nguyen, S. M., Wohlschlegel, J. A. and Hill, K. L. (2011). Independent analysis of the flagellum surface and matrix proteomes provides insight into flagellum signaling in mammalian-infectious *Trypanosoma brucei*. *Mol. Cell. Proteomics* **10**, M111.010538.
Portman, N., Lacomble, S., Thomas, B., McKean, P. G. and Gull, K. (2009). Combining RNA interference mutants and comparative proteomics to identify protein components and dependences in a eukaryotic flagellum. *J. Biol. Chem.* **284**, 5610-5619.
Ralston, K. S. and Hill, K. L. (2008). The flagellum of *Trypanosoma brucei*: new tricks from an old dog. *Int. J. Parasitol.* **38**, 869-884.
Robinson, D. R., Sherwin, T., Ploubidou, A., Byard, E. H. and Gull, K. (1995). Microtubule polarity and dynamics in the control of organelle positioning, segregation, and cytokinesis in the trypanosome cell cycle. *J. Cell Biol.* **128**, 1163-1172.
Rotureau, B., Blisnick, T., Subota, I., Julkowska, D., Cayet, N., Perrot, S. and Bastin, P. (2014). Flagellar adhesion in *Trypanosoma brucei* relies on interactions between different skeletal structures in the flagellum and cell body. *J. Cell Sci.* **127**, 204-215.
Schimanski, B., Nguyen, T. N. and Gunzl, A. (2005). Highly efficient tandem affinity purification of trypanosome protein complexes based on a novel epitope combination. *Eukaryot. Cell* **4**, 1942-1950.
Sun, S. Y., Wang, C., Yuan, Y. A. and He, C. Y. (2013). An intracellular membrane junction consisting of flagellum adhesion glycoproteins links flagellum biogenesis to cell morphogenesis in *Trypanosoma brucei*. *J. Cell Sci.* **126**, 520-531.
Sunter, J. D., Varga, V., Dean, S. and Gull, K. (2015). A dynamic coordination of flagellum and cytoplasmic cytoskeleton assembly specifies cell morphogenesis in trypanosomes. *J. Cell Sci.* **128**, 1580-1594.
Vaughan, S., Kohl, L., Ngai, I., Wheeler, R. J. and Gull, K. (2008). A repetitive protein essential for the flagellum attachment zone filament structure and function in *Trypanosoma brucei*. *Protist* **159**, 127-136.
Wei, Y., Hu, H., Lun, Z. R. and Li, Z. (2014). Centrin3 in trypanosomes maintains the stability of a flagellar inner-arm dynein for cell motility. *Nat. Commun.* **5**, 4060.
Wirtz, E., Leal, S., Ochatt, C. and Cross, G. A. M. (1999). A tightly regulated inducible expression system for conditional gene knock-outs and dominant-negative genetics in *Trypanosoma brucei*. *Mol. Biochem. Parasitol.* **99**, 89-101.
Woods, K., Nic a'Bhaird, N., Dooley, C., Perez-Morga, D. and Nolan, D. P. (2013). Identification and characterization of a stage specific membrane protein involved in flagellar attachment in *Trypanosoma brucei*. *PLoS ONE* **8**, e52846.
Zhou, Q., Gheiratmand, L., Chen, Y., Lim, T. K., Zhang, J., Li, S., Xia, N., Liu, B., Lin, Q. and He, C. Y. (2010). A comparative proteomic analysis reveals a new bi-lobe protein required for bi-lobe duplication and cell division in *Trypanosoma brucei*. *PLoS ONE* **5**, e9660.
Zhou, Q., Liu, B., Sun, Y. and He, C. Y. (2011). A coiled-coil- and C2-domain-containing protein is required for FAZ assembly and cell morphology in *Trypanosoma brucei*. *J. Cell Sci.* **124**, 3848-3858.